Quantitative Analysis of Hypertrophic Myocardium using Diffusion Tensor Magnetic Resonance Imaging

by

Nicholas Tran

THESIS

Submitted in partial satisfaction of the requirements for the degree of

MASTER OF SCIENCE

in

Biomedical Imaging

in the

GRADUATE DIVISION

of the

UNIVERSITY OF CALIFORNIA, SAN FRANCISCO

Acknowledgements

National Institutes of Health RO1 (1R01EB07219-01A1)

"Molecular Imaging of Cardiac Hypertrophy Using microPET and Pinhole SPECT"

Edward Hsu (University of Utah)

Michael Miller (Johns Hopkins University)

Archontis Giannakidis (Imperial College, London)

Damien Rohmer

Quantitative Analysis of Hypertrophic Myocardium using Diffusion Tensor Magnetic Resonance Imaging
Nicholas Tran

Abstract

Systemic hypertension is a causative factor in left ventricular hypertrophy which has a range of co-morbidities. Pathologic hypertrophy may negatively impact essential cardiac function. Understanding the physical and biomechanical changes in the heart associated with hypertensive left ventricular hypertrophy is motivated by the potential to reverse or manage the dysfunction associated with structural remodeling of the myocardium in this pathology. Diffusion tensor imaging is a nondestructive magnetic resonance imaging technique that can be used to image myocardial tissue microstructure and determine the orientation of myocardial muscle fibers. In this study, we present an analysis of myocardial fiber and laminar sheet orientation using the covariance of the diffusion tensor to quantify changes in orientation associated with myocardial tissue remodeling. We performed an *ex vivo* evaluation of hypertrophic and normal rat hearts (N=11) using diffusion tensor magnetic resonance imaging. We observed that the hypertrophic myocardium exhibited significantly increased myocardial fiber derangement (p=0.033), having a mean dispersion of 40 degrees. In comparison, normotensive myocardium had a mean of 36 degrees of dispersion. The calculated dispersion of the laminar sheet normal in the wild-type population was 52 degrees, compared to 55 degrees in the hypertrophic population (p=0.056). The fiber orientation distribution and dispersion data we obtained could be used to further evaluate the biomechanics of myocardial hypertrophy.

TABLE OF CONTENTS

LIST OF FIGURES

LIST OF TABLES

Introduction

Pathological ventricular hypertrophy is a myocardial condition that can arise from chronic systemic hypertension and is associated with oxidative stress, ischemia, and heart failure [1, 2, 3]. In previous studies, histology of the hypertrophic myocardium has demonstrated increased derangement of myocardial fibers [4, 5]. Reduced systolic and diastolic function associated with left ventricular hypertrophy may be a result of this myocardial fiber derangement and associated pathologies such as myocardial fibrosis. While the exact cause(s) of myocardial fiber disarray remain controversial [5], analysis of the myocardial microstructure and microstructural changes as a result of hypertension-associated structural remodeling may contribute to a better understanding of the biomechanics and electrical behavior of the pathologic myocardium [6] and help guide treatment of left ventricular hypertrophy.

Traditionally, assessments of myocardial fiber directionality have been performed histologically using tissue slices. This technique is destructive and sensitive to errors in slide preparation. Diffusion tensor magnetic resonance imaging (DTMRI, or simply DTI), is a magnetic resonance imaging technique that is sensitive to the anisotropic diffusion of water in tissue. The sensitivity of DTI to tissue anisotropy allows for non-destructive elucidation of myocardial tissue structure and can be extended to *in vivo* studies. The diffusion tensor, a 3×3 symmetric matrix at each voxel in a 3D volume, can be estimated using 6 or more diffusion-sensitizing gradient MR images and represents the diffusivity of water at the voxel [7]. Microstructural elements of the tissue, such as myocardial fibers, will

inhibit the water diffusion in an anisotropic manner [4,7]. It has been shown in studies correlating DTI and tissue histology that the primary eigenvector of the diffusion tensor is oriented with the myocardial muscle fiber, while the tertiary eigenvector is aligned with the laminar sheet normal [8]. Thus, the directionality of the myocardial fibers can be established nondestructively using DTI.

Since *in vivo* cardiac DTI is difficult due to cardiac motion, a model of the hypertrophic heart is required for *ex vivo* imaging. *Ex* vivo imaging of the healthy human heart is difficult due to the high demand for viable human hearts for transplantation, presenting the problem of obtaining an experimental control. The spontaneous hypertensive (SHR) rat serves as a model for systemic hypertension [9]. These rats develop left ventricular hypertrophy in response to chronic hypertension [9]. We present a voxel-wise comparative analysis of the myocardium in these rats to their normotensive controls, Wistar Kyoto (WKY) rats [10].

Materials and Methods:

Imaging Protocol

Diffusion tensor images from the hearts of 6 WKY and 6 SHR rats were collected over a span of 2 years, from 2009 to 2011. Isoflurane was used to anesthetize the rats, followed by removal of the heart, saline flush, and storage in formaldehyde solution prior to imaging. The ratios of heart/body masses were also obtained in order to confirm the presence of left ventricular hypertrophy. Diffusion tensor imaging was performed using a 12 gradient orientation, 3D spin-echo sequence with a TR/TE of 500/19.224ms and total acquisition time of 17 hours,

nominal b-value of 1000s/mm^2, for each data set using a Bruker BioSpec 7T small-animal scanner at the University of Utah. Image matrix size varied from 160×96×96 to 169×97×97 with constant voxel dimensions of 0.156×0.156×0.156 mm^3. Following data acquisition, diffusion tensor estimation was performed on the resultant diffusion-weighted imaging data sets using the nonlinear least-squares fitting algorithm [19].

Image Registration

In order to compare the microstructural differences voxel-by-voxel between the hypertrophic and control hearts, a standard normotensive heart atlas is needed as a reference. We chose to construct an atlas using group-wise registration of the WKY heart data, to which every data set from both SHR and WKY hearts would be registered. The diffusion tensor data set and unweighted anatomical image for each heart were cropped to an image matrix of 160×96×96 and voxel dimensions of 0.156×0.156×0.156 mm^3 in the Diffeomap software package developed by Johns Hopkins University. Registration of the diffusion tensor data was then performed based on the unweighted (b0) anatomical MRI images using the GLIRT iterative group-mean registration software package from the University of North Carolina-Chapel Hill [11]. Raw data of the anatomic image for each heart were converted to an 8-bit grayscale image in the Analyze format using a custom Matlab implementation. The resultant data were used as an input for GLIRT, which uses an iterative diffeomorphic demons transformation algorithm [12] to produce a group mean image.

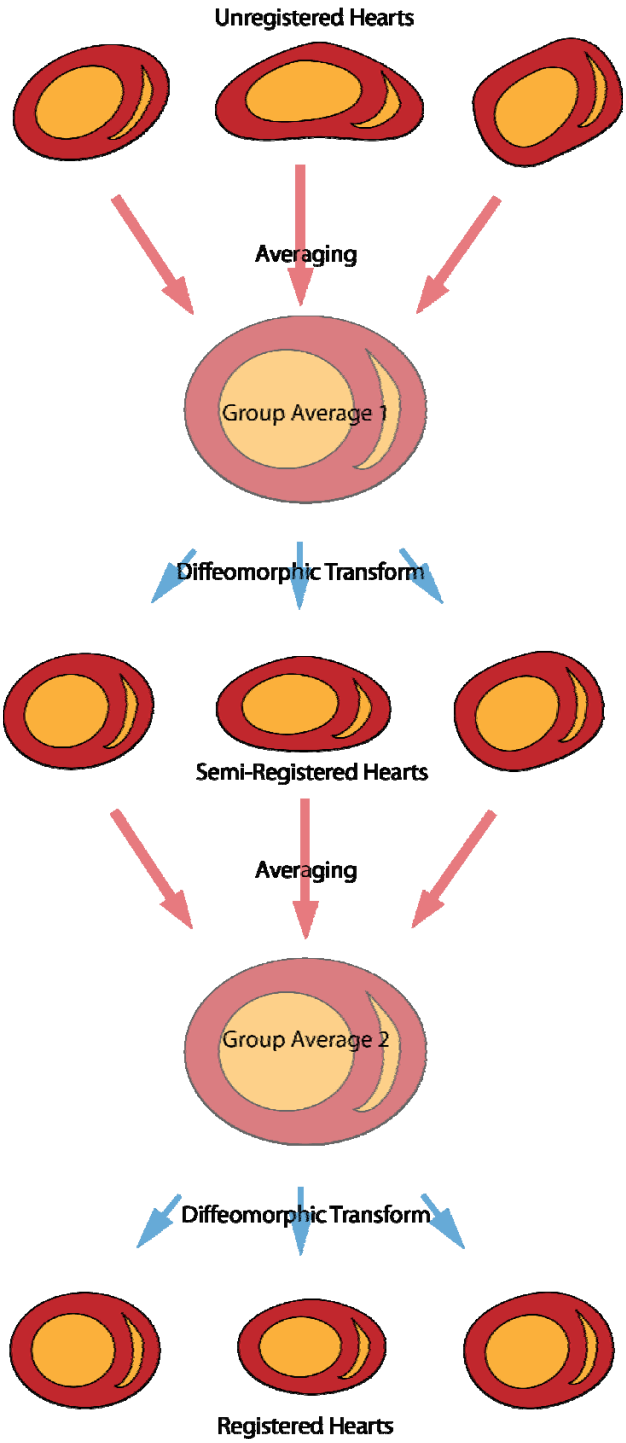

Figure 1: Iterative diffeomorphic registration used to produce group mean image.

GLIRT first computes a working group average from the unregistered hearts. This working average is used as the template to compute the first diffeomorphic transform of the hearts. A second working average is then taken of the transformed hearts, and is used as the template image for a second diffeomorphic transform (see Fig. 1). This process is iterated until the group average converges, which required 10 iterations. The Jaccard similarity between the thresholded 9^{th} and 10^{th} was calculated to be 1, and convergence verified by visual inspection.

As part of the process of creating the group mean average, GLIRT created registered versions of the input WKY hearts. In order to register both populations using identical methods, however, the resulting final group mean image was then used as the reference image to which the SHR and WKY hearts were co-registered. Automatic registration was performed using the Diffeomap and DTIstudio software packages from Johns Hopkins University [13]. A landmark-based affine transformation (df=12) was first used, with the apex of the heart, papillary muscles, and right ventricle chamber as the reference points. After manual histogram intensity matching was performed on each anatomical image, the automatic LDDMM (Large Deformation Diffeomorphic Metric Mapping) function of Diffeomap was used to compute the final registration [13], and the resulting deformation fields were used to transform the diffusion tensor data of each heart. Tensor reorientation was performed using the Preservation of Principal Direction strategy [14]. The myocardium was segmented using a global threshold and the Jaccard similarity coefficient, calculated by dividing the intersection of two sample sets by their union, was obtained using Matlab for each sample heart with the group mean to assess the

quality of registration [15]. The coefficient varies between 0 for two sets that do not intersect at all and 1 for sets that are identical.

Table 1: Jaccard similarity coefficients for registered wild-type hearts.

Sample	WKY1	WKY3	WKY4	WKY6	WKY8
Similarity	.9072	.9474	.9158	.8896	.8959

Table 2: Jaccard similarity coefficients for registered hypertrophic hearts.

Sample	SHR1	SHR2	SHR3	SHR4	SHR6	SHR8
Similarity	.7879	.7679	.7393	.8401	.7990	.8478

This registered diffusion tensor data were used to compute an average tensor atlas for the normal WKY rat heart. Since the registered tensor data now share spatial and anatomical coordinates, a voxel-wise comparison can be drawn between the hypertrophic rat hearts and the normotensive WKY type.

Log-Euclidean Tensor Averaging

Following registration, an average WKY tensor image was computed using the WKY tensor image data. Due to the non-Euclidean nature of the diffusion tensor, Euclidean element-wise averaging of the tensor at each voxel produces inaccurate results [16], which can lead to misleadingly inflated diffusivity. Tensor averaging was implemented in Matlab following the Log-Euclidean framework, which is a computationally efficient system that avoids these problems of tensor swelling and asymmetry.

Since the diffusion tensor is by definition symmetric positive-definite, its matrix logarithm can be computed by diagonalizing the tensor:

$$D = R^T S R \qquad (1).$$

where *D*, the diffusion tensor, is decomposed into the rotation matrix *R*, and *S*, the matrix containing the tensor eigenvalues along the diagonal. *S'* is then computed by taking the natural logarithm of each of the eigenvalues:

$$S'_{(i,i)} = \log(S_{(i,i)}) \quad (2) \text{ for } i = 1,2,3.$$

The matrix logarithm at a given voxel is then:

$$\log(D) = R^T S' R \qquad (3).$$

The mean tensor can then be calculated by averaging the tensor logarithms voxel-wise across *N* tensor images and taking the matrix exponent [16]:

$$\overline{D}(x) = \exp(\frac{1}{N}\sum_{i=1}^{N}\log(D_i(x))) \qquad (4).$$

This computation was performed voxel-wise across a 160×96×96 image matrix size using all the WKY tensor data after image registration. Following this, the dispersion measures (discussed at length below) were computed on each WKY heart to identify outliers. One WKY heart was excluded from the data set due to high dispersion measures falling >2 standard deviations above the average, and the mean tensor recalculated using the remaining 5 hearts. The result of this was the WKY heart tensor atlas that will serve as the basis of the tensor dispersion comparison.

Myocardial Dispersion Measures

The covariance matrix between each tensor and the average tensor was then computed, again using a custom-written Matlab implementation. Compared to scalar DTI measures such as the fractional anisotropy (FA), the covariance method

describes the variability in orientation of the tensor about some reference rather than the simple magnitude of the anisotropy. This information allows differences in myocardial fiber directionality to be comparatively analyzed potentially providing greater insight than can be obtained from the orientation-invariant intra-voxel information provided by FA. The covariance Σ between the tensor D and the mean tensor $\overline{D}(x)$ is given by the following [17]:

$$\Delta D(x) = \log(D) - \log(\overline{D}(x)) \quad (5),$$

$$vec(D) = [D_{(1,1)}, \sqrt{2}D_{(1,2)}, D_{(2,2)}, \sqrt{2}D_{(1,2)}, \sqrt{2}D_{(3,1)}, \sqrt{2}D_{(3,2)}, D_{(3,3)}] \quad (6), \text{ and}$$

$$\Sigma(x) = vec(\Delta D(x)) \cdot vec(\Delta D(x))^T \quad (7).$$

At a given voxel, the components of the 6x6 covariance matrix in Eq. 7, in the directions of the planes normal to the 3 eigenvectors of the mean tensor, correspond to the dispersions of the 3 equivalent eigenvectors of the sample tensor D. Thus, the orthonormal basis of the mean diffusion tensor is computed (Eqs. 8-10), with the motivation of projecting the covariance matrix on to the appropriate directions to compute the eigenvector variability.

$$W_{2,3} = \frac{1}{\sqrt{2}}(v_3 \cdot v_2^T + v_2 \cdot v_3^T) \quad (8),$$

$$W_{1,3} = \frac{1}{\sqrt{2}}(v_3 \cdot v_1^T + v_3 \cdot v_1^T) \quad (9), \text{ and}$$

$$W_{1,2} = \frac{1}{\sqrt{2}}(v_2 \cdot v_1^T + v_1 \cdot v_2^T) \quad (10),$$

where v_i ,for i = 1,2,3, are the three eigenvectors of the mean tensor.

The 3 planes defined by sets of these orthonormal vectors $W_{i,j}$ correspond to the 3 planes normal to the eigenvectors of the average tensor. By computing the components of the covariance matrix in these planes the variability of the tensor eigenvectors about the average eigenvectors can be calculated [17] by

$$E(\varepsilon_{23}{}^2) = \frac{1}{2(\lambda_2 - \lambda_3)^2}(vec(W_{2,3})^T \cdot \Sigma \cdot vec(W_{2,3})) \qquad (11),$$

$$E(\varepsilon_{13}{}^2) = \frac{1}{2(\lambda_1 - \lambda_3)^2}(vec(W_{1,3})^T \cdot \Sigma \cdot vec(W_{1,3})) \qquad (12), \text{ and}$$

$$E(\varepsilon_{12}{}^2) = \frac{1}{2(\lambda_1 - \lambda_2)^2}(vec(W_{1,2})^T \cdot \Sigma \cdot vec(W_{1,2})) \qquad (13)$$

where $\lambda_i = \log(d_i)$ and d_i are the eigenvalues of the mean tensor in the log and Euclidean spaces, respectively, and i = 1,2,3.

Equations 11-13 correspond to the dispersion of the myocardial laminar sheet and myocardial fibers about the average where ε_{ij} represents the tangent of the angle of the eigenvector about the mean [17]. By taking the inverse tangent, the angular variability of the sample tensor eigenvectors about the mean can be obtained. One can imagine this as a set of cones of uncertainty surrounding each of the mean eigenvectors. The dispersion about the primary eigenvector describes the variability of the myocardial fiber. The dispersion about the tertiary eigenvector describes the variability of the laminar sheet normal. This method was generalized to compare multiple tensors D to the mean, obtaining dispersion measures for each heart in the WKY and SHR populations.

Results

The dispersion of the myocardial fibers about the normal average provide insight into the remodeling of the myocardium in hypertrophy. The magnitude of the angular dispersion about the primary eigenvector describes the variability of the myocardial fiber orientation. The spatial distribution of this variability can be assessed by mapping the angular dispersion as shown in Figure 2.

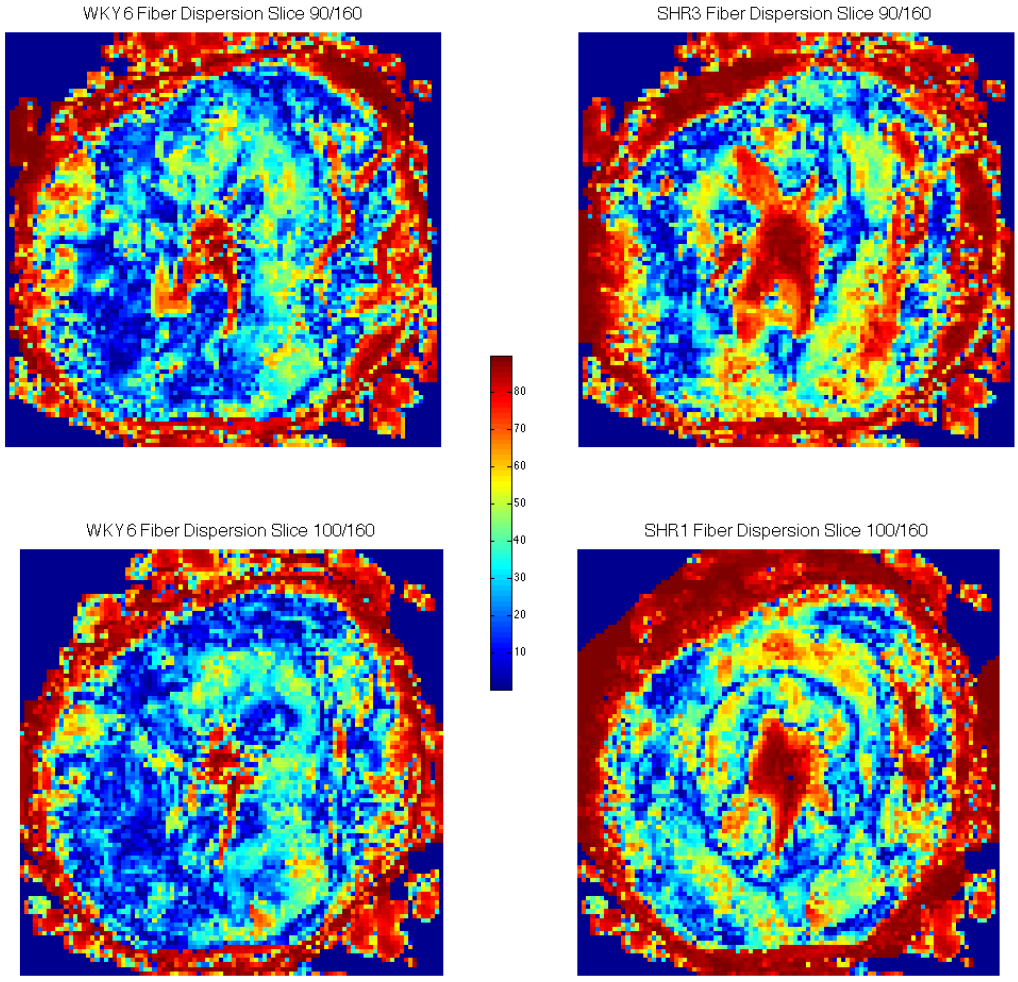

Figure 2: Unmasked myocardial fiber dispersion map for selected axial slice through selected WKY (left) and SHR (right) hearts. Cooler colors indicate lower dispersion while warm colors indicate high dispersion (Values in degrees).

Visual inspection of these dispersion maps suggests that the hypertrophic hearts have a higher degree of angular dispersion than the normotensive hearts. To confirm this, the mean fiber variability was calculated for each heart. In order to exclude low-signal edge voxels, each dataset was first masked using the thresholded anatomical group mean image shown in Figure 3.

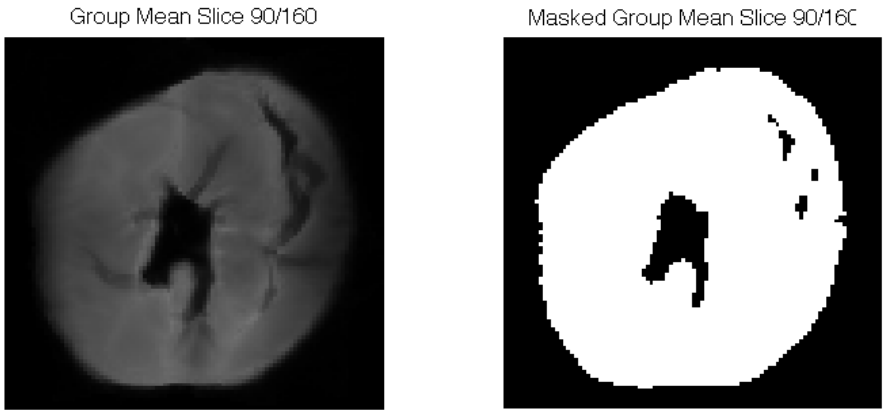

Figure 3: Greyscale and thresholded group mean image for selected short axis slice.

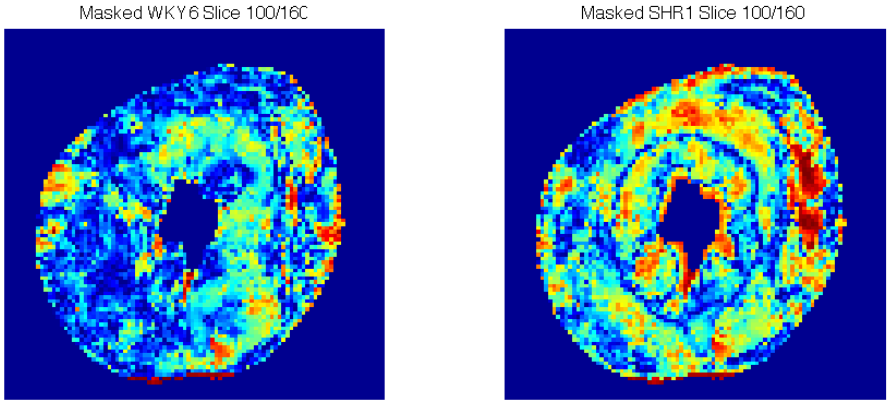

Figure 4: Masked myocardial fiber dispersion maps for selected WKY and SHR hearts, selected short-axis slice.

An example of the masked dispersion maps used to calculate overall statistics is presented in Figure 4.

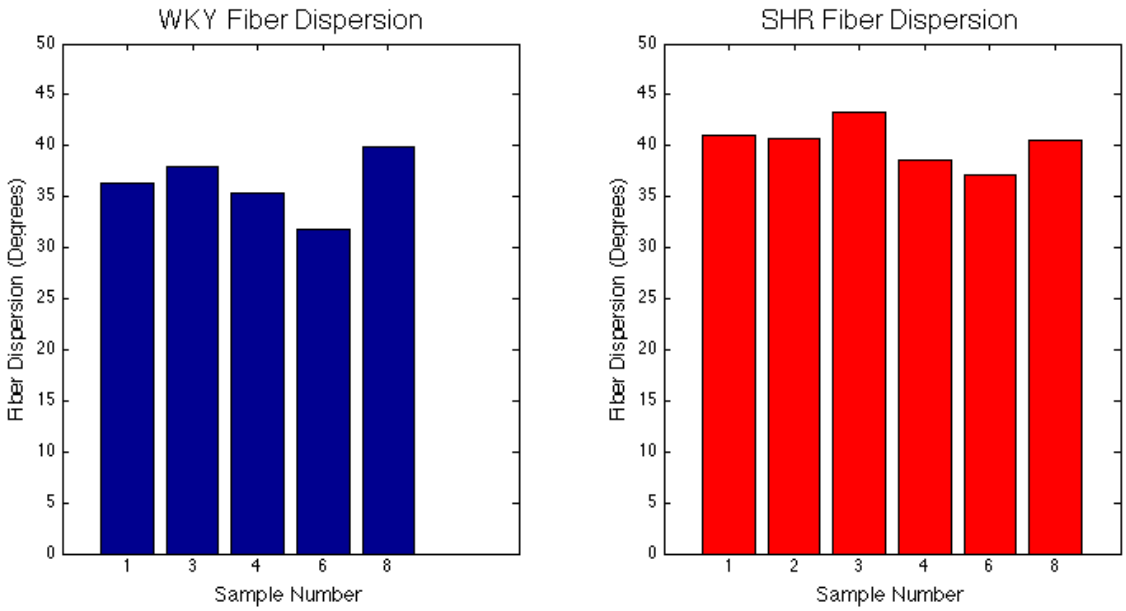

Figure 5: Mean myocardial fiber dispersion for each WKY and SHR heart, measured in degrees. WKY hearts are presented in blue, SHR in red.

As observed in Figure 5, the mean fiber dispersion is higher in the hypertrophic hearts than in the normotensive hearts, with some intrapopulation variation. The average fiber dispersion across all wild-type hearts was 36 degrees. This was lower than the average fiber dispersion for the hypertrophic hearts, which had an overall mean of 40 degrees of dispersion. The p-value obtained using a two-tailed *t*-test was 0.033.

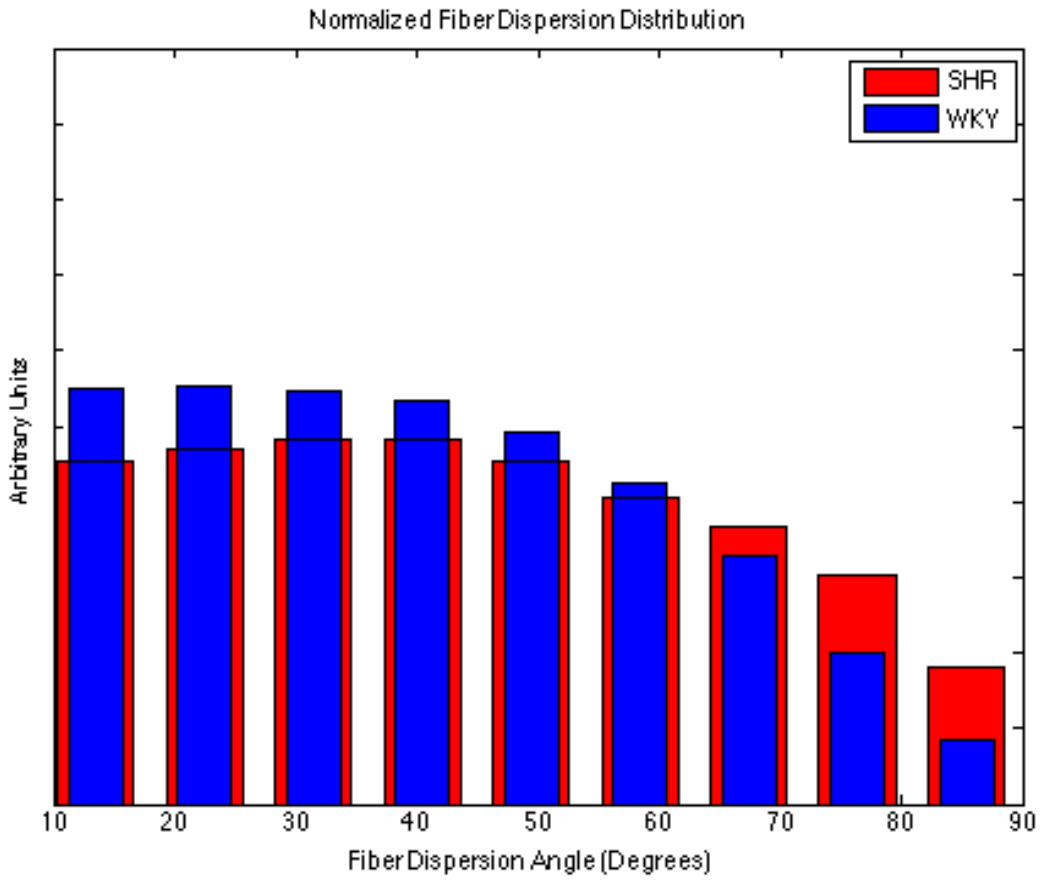

Figure 6: Histogram of myocardial fiber dispersion angles for WKY and SHR hearts, measured in degrees.

An overall voxel distribution of myocardial fiber angles was also plotted for the normal WKY and hypertrophic hearts in Fig. 6, normalized by dividing each bin count by the total number of voxels for the corresponding population. The histogram shows an increased proportion of high-dispersion voxels in the hypertrophic population compared to the normal type.

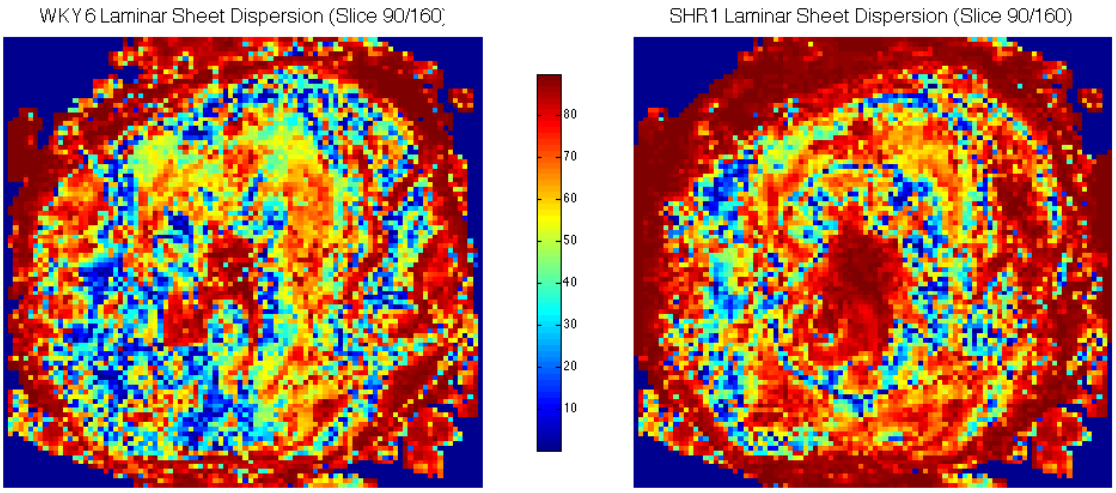

Figure 7: Unmasked laminar sheet dispersion map for selected axial slice through selected WKY (left) and SHR (right) hearts. Cool colors indicate low dispersion, while warm colors indicate higher dispersion (Values in degrees).

This same data analysis can be performed on the dispersion measures of the laminar sheet (that is, the covariance about the third diffusion tensor eigenvector). These measures show increased variability compared to the primary eigenvector (see Fig. 7).

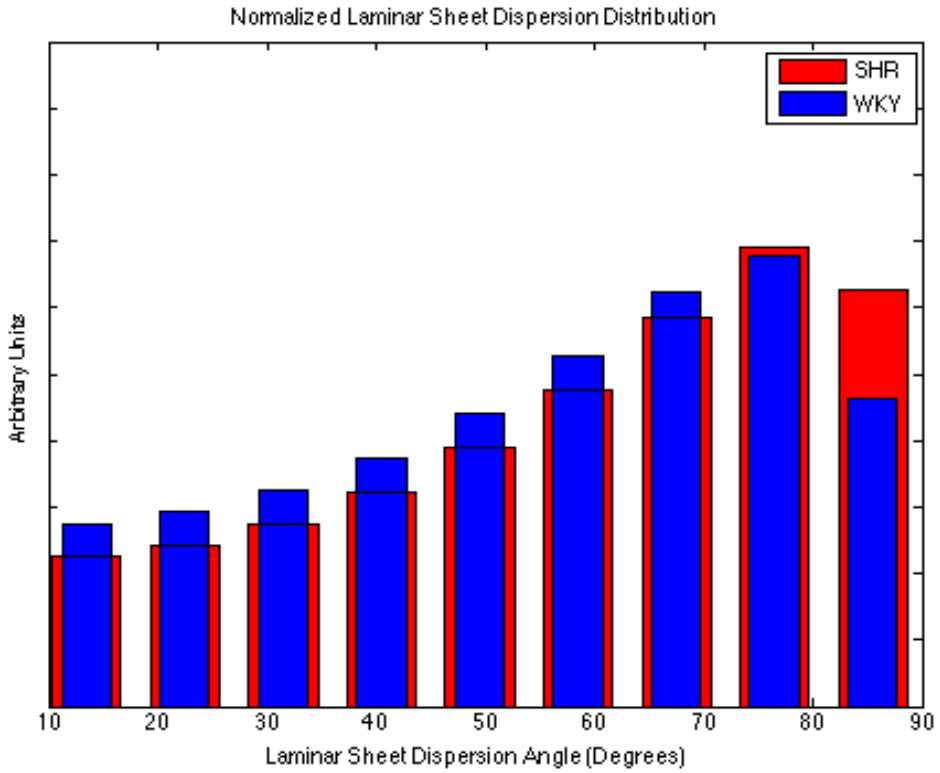

Figure 8: Histogram of laminar sheet dispersion angles for WKY and SHR hearts, measured in degrees.

As with the fiber orientation dispersion, the comparative difference between WKY and SHR populations is mirrored in the analysis of the laminar sheet angular dispersion, with characteristic increased dispersion in the hypertrophic population shown in Fig. 8. The calculated dispersion of the laminar sheet normal in the wild-type population was 52 degrees, compared to 55 degrees in the hypertrophic population. The p-value obtained using a two-tailed *t*-test was 0.056.

Discussion

We observed a statistically significant difference in the myocardial fiber dispersion between the normal wild-type and the hypertrophic populations ($p < 0.05$). Left ventricular hypertrophy has been correlated with increased fibrosis and impaired systolic and diastolic function in patients recovering from myocardial infarction [3]. Analysis of myocardial tissue microstructure and myocardial fiber orientation may reveal the underlying biomechanical changes that result in reduced myocardial function, as the increased myocardial fiber disarray observed in this study may be an indicator or causative factor of reduced cardiac function. Computer simulation of the left ventricle using the myocardial fiber distributions and dispersion data obtained in this study may be useful in understanding the biomechanical ramifications of left ventricular hypertrophy [18].

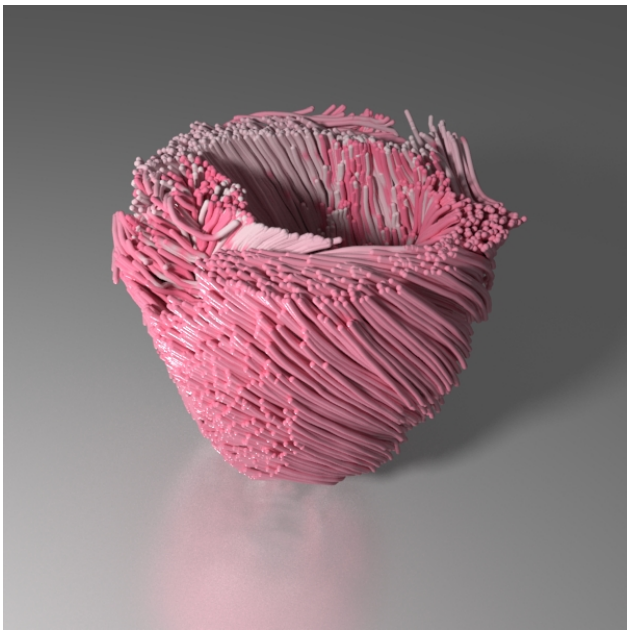

Figure 9: Render of fiber-tracking results from DT-MRI data (Courtesy Damien Rohmer).

Visualization of diffusion tensor data has been explored using fiber-tracking methods [18]. This reconstruction and visualization technique, shown in Figure 9, does not currently incorporate fiber orientation variability. Fusion of the dispersion measures obtained in this study and fiber-tracking results from the corresponding diffusion tensor data is a future project that could provide further insight into the spatial localization of the pathology and its impact on heart function.

This study was limited by its small sample size and registration quality. It is possible that the observed dispersion difference between the wild-type normal and hypertrophic hearts arose due to the lower quality of registration for the hypertrophic hearts, possibly due to gross anatomical differences between the hypertrophic and normotensive populations. We noted a statistically significant (p<.05) difference between the Jaccard similarity coefficients (Tables 1 & 2) for the WKY and SHR populations due in part to anatomical variations in the two populations. Since differences in orientation can affect the anatomical group average, which was generated *prior* to performing the affine transform, inconsistency in the image acquisition can reduce the overall quality of the subsequently computed tensor atlas, negatively affecting the quality of the analysis. Despite these limitations, statistically significant differences were observed in the myocardial fiber dispersion measures between the wild-type and hypertrophic populations, which is consistent with previous histological studies [5].

Conclusion

Our results demonstrate significantly increased myocardial muscle fiber and laminar sheet disarray in rats that suffer from hypertensive left ventricular hypertrophy. The dispersion data obtained can be combined with fiber-tracking methods [10, 18] to visualize myocardial changes in ventricular hypertrophy as well as create muscle fiber distributions for biomechanical computer modeling [10] of the hypertrophic heart.

References:

[1] Alvarez, M.C.; Caldiz, C.; Fantinelli, J.C.; Garciarena, C.D.; Console, G.M.; Chiappe de Cingolani, G.E.; Mosca, S.M. Is Cardiac Hypertrophy in Spontaneously Hypertensive Rats the Cause or the Consequence of Oxidative Stress? *Hypertens Res.* **2008** 31(7):1465-74.

[2] Breslin, D.J.; Gifford, R.W.; Fairbairn, J.F. Essential Hypertension: A Twenty-Year Follow-Up Study. *Circulation.* **1966** 33:87-97

[3] Kaplinsky, E. Significance of elft ventricular hypertrophy in cardiovascular morbidity and mortality. *Cardiovasc Drugs Ther.* **1994** 8 Suppl 3:549-56.

[4] Bulkley, B.H.; Weisfeldt, M.L.; Hutchins, G.M. Asymmetric septal hypertrophy and myocardial fiber disarray: Features of normal, developing, and malformed hearts. *Circulation.* **1977** 56(2):292-8.

[5] St. John Sutton, M.G.; Lie, J.T.; Anderson, K.R.; O'Brien, P.C.; Frye, R.L. Histopathological specificity of hypertrophic obstructive cardiomyopathy. *Br Heart J* **1980** 44:433-43.

[6] Hsu, E.W.; Muzikant, A.L.; Matulevicius, S.A.; Penland, R.C.; Henriquez, C.S. Magnetic resonance myocardial fiber-orientation mapping with direct histological correlation. *Am J Physiol.* **1998** 274(5 Pt 2):H1627-34.

[7] Basser, P.J.; Mattiello, J.; LeBihan, D. Estimation of the Effective Self-Diffusion Tensor from the NMR Spin Echo. *J Magn Reson.* **1994** 103(3):247-54.

[8] Helm, P.A.; Tseng, H.J.; Younes, L.; McVeigh, E.; Winslow, R.L. Ex Vivo 3D Diffusion Tensor Imaging and Quantification of Cardiac Laminar Structure. *Magn Reson Med.* **2005** 54(4):850-9.

[9] Sen, S.; Tarazi, R.C.; Khairallah, P.A.; Bumpus, F.M. Cardiac Hypertrophy in Spontaneously Hypertensive Rats. *Circ Res.* **1974** 35:775-81.

[10] Giannakidis, A.; Rohmer, D.; Veress, A.I.; Gullberg, G.T. Diffusion Tensor Magnetic Resonance Imaging-Derived Myocardial Fiber Disarray in Hypertensive Left Ventricular Hypertrophy: Visualization, Quantification, and the Effect on Mechanical Function. *Cardiac Mapping.* Wiley: London, **2012,** 574-588

[11] Wu, G.; Wang, Q.; Shen, D. Registration of Longitudinal Image Sequences with Implicit Template and Spatial-Temporal Heuristics. *NeuroImage.* **2012** 59(1):404-12.

[12] Vercauteren, T.; Pennec, X.; Perchant, A.; Ayache, N. Diffeomorphic demons: Efficient non-parametric image registration. *Neuroimage*. **2008** 45(1):S61-S72.

[13] Beg, F.; Miller, M.I.; Trouve, A.; Younes, L. Computing Large Deformation Metric Mappings via Geodesic Flows of Diffeomorphisms. *International Journal of Computer Vision*. **2005** 61(2):139-57.

[14] Alexander, D.; Pierpaoli, C., Basser, P.; Gee, J.C. An Algorithm for Preservation of Orientation during Non-Rigid Warps of Diffusion Tensor Magnetic Resonance (DT-MR) Images. *Proc. Intl. Soc. Mag. Reson. Med* **2001** 9:791.

[15] Klein, A.; Andersson, J.; Ardekani, B.A.; Ashburner, J.; Avants, B.; Chiang, M.C.; Christensen, G.E.; Collins, D.L.; Gee, J.; Hellier, P.; Song, J.H.; Jenkinson, M.; Lepage, C.; Ruechert, D.; Thompson, P.; Vercauteren, T.; Woods, R.P.; Mann, J.J.; Persey, R.V. Evaluation of 14 nonlinear deformation algorithms applied to human brain MRI registration. *Neuroimage* **2009** 46(3):786-802.

[16] Arsigny, V.; Fillard, P.; Pennec, X.; Ayache, N. Fast and Simple Calculus on Tensors in the Log-Euclidean Framework. *Magn Reson Med.* **2006** 56(2):411-21.

[17] Peyrat, J.M.; Sermesant, M.; Pennec, X.; Delingette, H.; Xu, C.; McVeigh, E.; Ayache, N. A Computational Framework for the Statistical Analysis of Cardiac Diffusion Tensors: Application to a Small Database of Canine Hearts. *IEEE Trans Med Imag.* **2007** 26(1):1500-13.

[18] Rohmer, D.; Sitek, A.; Gullberg, G.T. Reconstruction and Visualization of Fiber and Laminar Structure in the Normal Human Heart from Ex Vivo Diffusion Tensor Magnetic Resonance Imaging (DTMRI) Data. *Invest Radiol*. **2007** 42(11):777-89.

[19] Koay, C.G.; Chang, L.C.; Carew, J.D.; Pierpaoli, C.; Basser, P.J. A unifying theoretical and algorithmic framework for least squares methods of estimation in diffusion tensor imaging. *J Magn Reson* **2006**182:115–25.

Publishing Agreement

It is the policy of the University to encourage the distribution of all theses, dissertations, and manuscripts. Copies of all UCSF theses, dissertations, and manuscripts will be routed to the library via the Graduate Division. The library will make all theses, dissertations, and manuscripts accessible to the public and will preserve these to the best of their abilities, in perpetuity.

Please sign the following statement:

I hereby grant permission to the Graduate Division of the University of California, San Francisco to release copies of my thesis, dissertation, or manuscript to the Campus Library to provide access and preservation, in whole or in part, in perpetuity.

Author Signature

8/26/2014

Date